Effects of Processing and Drug Loading on Morphology and Drug Release in PCL–Rifampicin Systems

By

Susan George

Biomedical Engineering, B.Eng, Stevens Institute of Technology, 2023

Thesis

Submitted in partial fulfillment of the requirements for the Degree of Master of Science in the Graduate program of Biotechnology at Brown University

PROVIDENCE, RHODE ISLAND

MAY 2026

This thesis by SUSAN GEORGE is accepted in its present form by the Graduate Program in Biotechnology as satisfying the thesis requirements for the degree of Master of Science

Date 4/28/2026 Signature: DocuSigned by: EDITH MATHIOWITZ E063C09A6AB6428...

Dr. EDITH MATHIOWITZ, Advisor

Date 4/22/2026 Signature: DocuSigned by: Eric Darling 46DB889F981A404...

Dr. ERIC DARLING, Reader

Date 4/23/2026 Signature: DocuSigned by: Yong Jong 6BE6ACE763A2447...

Dr. YONG JONG, Reader

Approved by the Graduate Council

Date _____ Signature: _____

Dr. David P. Lindstrom, Dean of the Graduate School

Acknowledgements:

First, I would like to thank my advisor, Dr. Edith Mathiowitz, for being an incredible mentor throughout my scientific journey and for supporting my academic, career, and personal growth. The kindness, knowledge, and wisdom you have shared with me during my time at Brown have been truly invaluable and will stay with me moving forward.

I would also like to thank my committee members, Dr. Eric Darling and Dr. Yong Jong, for their time, guidance, and thoughtful insight throughout this process. I feel especially fortunate to have learned from both of you in the classroom, where you introduced me to new concepts and deepened my understanding of the science industry. Additionally, thank you to Dr. Hector Garces for his help with the XRD.

I also extend my appreciation to Jingge Chen, Zakhar Lyakovych, and Anthony Comeau for their technical support and expertise throughout my project. A special thank you to my labmates turned friends: David Shafiei, Jelynn Tatad, and Floor Keuning, for their help with experiments, always being a sounding board, and helping me maintain my sanity along the way. I would also like to acknowledge the rest of the Mathiowitz lab for fostering such a collaborative and supportive environment: Anju Meda, Michael DeSantis, Liston Dsouza, Hena Haque, Tuyetanh Le, Danait Selamawi, Joel Fisher, Alex Lim, Oindrela Seha, and Sasha van Steenburgh.

Finally, to my friends, old and new, thanks for making Brown such an incredible experience, and to my family for their constant support throughout.

Table of Contents:

Table of Figures

Table of Tables

Abstract of Effects of Processing and Drug Loading on Morphology and Drug Release in PCL–Rifampicin Systems, by Susan George, ScM, Brown University, MAY 2026.

This study examines how processing conditions regulate polymer morphology and mesophase formation in poly(caprolactone) (PCL) and how these structural transitions govern rifampicin release behavior. Demonstrating that pressure and temperature-controlled processing induce mesophase formation in PCL and PCLRifampicin matrices.

PCLRifampicin matrices were fabricated via film casting (0–30% w/w drug loading) and subjected to processing at 22°C, 50°C, and 60°C under 10,000 lb of pressure. Morphological characterization using polarized light microscopy (PLM) and X-ray diffraction (XRD) was used to assess phase structure and chain organization. While Scanning Electron Microscopy (SEM) showed drug distribution within the polymer matrix.

PLM showed pressure-induced birefringence consistent with enhanced chain alignment and mesophase formation. XRD revealed a transition from sharp crystalline peaks to broadened diffuse scattering, indicating partial crystal disruption and increased mesomorphic ordering, most pronounced at 22°C and 50°C. At 60°C, recrystallization reduced mesophase content and restored crystalline dominance. In vitro release studies demonstrated that mesophase-rich, pressure processed samples exhibited slower, more sustained rifampicin release compared to filmcast controls, which showed pronounced burst release and rapid depletion. Higher mesophase content correlated with reduced cumulative drug release, reflecting decreased effective diffusivity through the more ordered polymer network.

This morphological control works to establish mesophase engineering as a mechanism for tuning sustained drug release in PCL systems.

Chapter 1: Introduction

Rifampicin:

Rifampicin (also known as rifampin) is a broad-spectrum antimicrobial agent widely used in the treatment of gram-positive and mycobacterial infections, including *Mycobacterium tuberculosis, Staphylococcus aureus,* and *Neisseria meningitidis*[1]. Its mechanism of action targets bacterial RNA synthesis, a process essential for cellular growth and replication. Specifically, rifampicin binds to the βsubunit of DNA-dependent RNA polymerase (RNAP), forming a stable drug–enzyme complex that blocks RNA chain elongation. This inhibition prevents RNA production and ultimately leads to bacterial cell death due to the inability to synthesize essential proteins. Importantly, this interaction is highly selective and does not affect RNA polymerase in human cells [2].

Clinically, rifampicin has been FDA-approved for the treatment of tuberculosis since 1971 and remains a cornerstone of antitubercular therapy. It is also used off-label for conditions such as leprosy, prosthetic joint infections (PJI), and severe gram-positive bacterial infections [3]. The global rifampicin market continues to grow, with 2025 revenue projected to reach approximately $14.68 billion, driven largely by the global tuberculosis burden, and is expected to exceed $24 billion by 2033[4]. Rifampicin is most commonly administered orally, although intravenous delivery may be used in more severe cases. In tuberculosis treatment, it is typically dosed at approximately 10 mg/kg over a six-month course. Despite its clinical efficacy, rifampicin is associated with adverse effects, including hepatotoxicity, hypersensitivity reactions, gastrointestinal disturbances, and neurological symptoms [5].

A major limitation of rifampicin therapy is the rapid emergence of resistance when used as a monotherapy, primarily due to mutations in the RNA polymerase target. Consequently,

rifampicin is almost always administered in combination with other antimicrobials, such as isoniazid, ethambutol, and pyrazinamide, to mitigate resistance development[6]. Pharmacokinetically, rifampicin exhibits an oral bioavailability of approximately 80-95%, which decreases when administered with food, and still requires relatively high doses to achieve therapeutic effects [7]. Furthermore, rifampicin undergoes concentration dependent autoinduction of its own metabolism, leading to reduced systemic exposure with repeated dosing. Its elimination half-life of approximately 2.5 hours further necessitates frequent administration in conventional treatment regimens [8].

From a physicochemical perspective, rifampicin is a hydrophobic molecule with a molecular weight of 822.94 g/mol and a melting point of 183–188 °C. It demonstrates high potency, with minimum inhibitory concentration (MIC) values for Mycobacterium tuberculosis typically ranging from 0.05–0.5 μg/mL[9]. While these properties contribute to its therapeutic effectiveness, they also present challenges in achieving sustained and localized drug exposure, particularly in complex infection environments. These limitations are especially pronounced in the treatment of prosthetic joint infections (PJI), where biofilm-forming organisms such as Staphylococcus aureus and Staphylococcus epidermidis create protective microenvironments that limit antibiotic penetration and efficacy. Although rifampicin is uniquely capable of penetrating biofilms and maintaining activity against metabolically quiescent bacteria, systemic administration often fails to achieve sufficient local concentrations while increasing the risk of systemic toxicity[7,10].

Drug Delivery:

Drug delivery systems are designed to facilitate the transport of active pharmaceutical ingredients within the body to achieve a desired therapeutic effect. These systems can be engineered to enhance drug efficacy, optimize pharmacokinetic profiles, and minimize off-target toxicity [11]. Over the past two decades, significant advances have been made in the development of controlled drug delivery systems to address the limitations of conventional dosage forms, including tablets [12], syrups [13], injections [14], and topicals [15], which often suffer from limited bioavailability and fluctuations in plasma drug concentrations that necessitate frequent dosing [16].

Controlled drug delivery systems are specifically designed to maintain drug concentrations within a defined therapeutic window over extended periods of time, ideally achieving a near-constant (non-zero-order) pharmacokinetic profile, as illustrated in Figure 1. By minimizing peak-trough fluctuations, these systems can improve therapeutic efficacy while reducing adverse effects associated with high systemic exposure. At their core, controlled delivery systems aim to improve patient outcomes by enhancing efficacy, reducing toxicity, and increasing patient compliance through reduced dosing frequency [17].

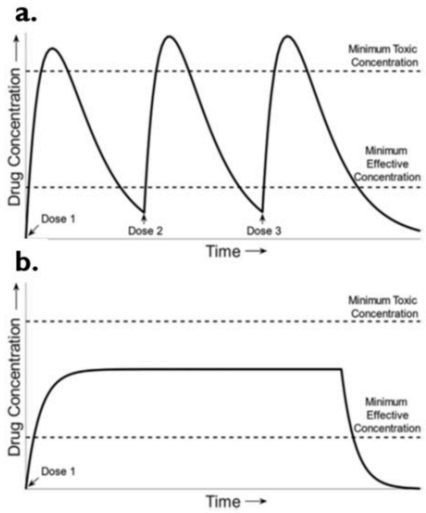

Figure 1: a. Conventional vs b. Controlled Drug Delivery System [17].

These advantages are particularly relevant for rifampicin. As noted, rifampicin is most commonly administered orally or intravenously in severe cases[18]. However, these administration routes require high-dose, long-term treatment regimens, which are associated with significant drawbacks. Prolonged exposure increases the risk of adverse effects such as hepatotoxicity, while treatment efficacy is often compromised by poor patient adherence over extended durations. Additionally, oral administration presents pharmacokinetic challenges, including variable absorption, reduced bioavailability due to autoinduction of metabolism, and difficulty maintaining consistent therapeutic drug levels [19].

Effective treatment of infections such as tuberculosis and PJI requires that rifampicin reach and maintain sufficient concentrations at the site of infection. In tuberculosis, this includes penetration into pulmonary tissue and granulomatous lesions, while in PJI, high local concentrations are required to eradicate biofilm-associated bacteria. Achieving and sustaining these concentrations through systemic delivery alone is challenging due to distribution limitations and restricted penetration into infected tissues[20].

As such, long-term controlled release systems represent a compelling strategy to overcome these limitations. Implantable drug delivery systems, in particular, offer a promising approach for rifampicin delivery. By enabling continuous and controlled release, implants can maintain consistent plasma concentrations, improve drug distribution to target tissues, and reduce pharmacokinetic variability. Furthermore, this approach is adaptable across multiple clinical contexts: subcutaneous implants may provide sustained systemic delivery for tuberculosis, while localized implants positioned at or near prosthetic joints may deliver high

drug concentrations directly to the site of infection, enhancing bacterial clearance while minimizing systemic exposure [21].

Polymers:

Polymers are large macromolecules composed of repeating monomer units and are integral to nearly every aspect of modern life, from clothing to construction materials. In pharmaceuticals and biomedicine, polymers have garnered significant interest due to their inherent tunability and versatility, enabling their use across a wide range of applications, including tissue engineering, biosensing, and drug delivery [22]. Broadly, polymers can be categorized as either natural or synthetic. Natural polymers, such as polysaccharides, are derived from biological systems and offer inherent biocompatibility and biodegradability, while synthetic polymers are engineered through polymerization processes and provide enhanced stability and manufacturability [23].

Within biomedical applications, biocompatibility is a critical consideration to ensure patient safety and therapeutic efficacy, while other material properties, such as biodegradability, are selected based on the intended application [24]. Biodegradable polymers such as PCL undergo degradation through hydrolytic or enzymatic mechanisms, with drug release governed by both diffusion and degradation kinetics. In contrast, nonbiodegradable polymers retain their structural integrity, resulting in drug release that is primarily diffusion driven [25].

Importantly, polymer properties, including mechanical strength, thermal behavior, and degradation profiles, can be systematically tuned through modifications in molecular weight, crystallinity, and chemical structure. This level of control enables the precise engineering of polymer-based drug delivery systems to optimize drug loading, modulate release kinetics, and achieve targeted delivery [26].

Mesophase

Polymers are generally classified as either amorphous or semicrystalline based on their internal structure. Amorphous polymers exhibit a random, isotropic arrangement of polymer chains, whereas semicrystalline polymers contain both disordered amorphous regions and ordered crystalline domains. These crystalline regions organize into spherulitic structures composed of radially arranged lamellae interconnected by amorphous phases [27]. Polymer morphology plays a critical role in determining material properties, including mechanical strength, degradation behavior, and diffusivity. Amorphous polymers tend to be more ductile and exhibit faster dissolution, whereas highly crystalline polymers are more rigid, mechanically robust, and resistant to degradation [28].

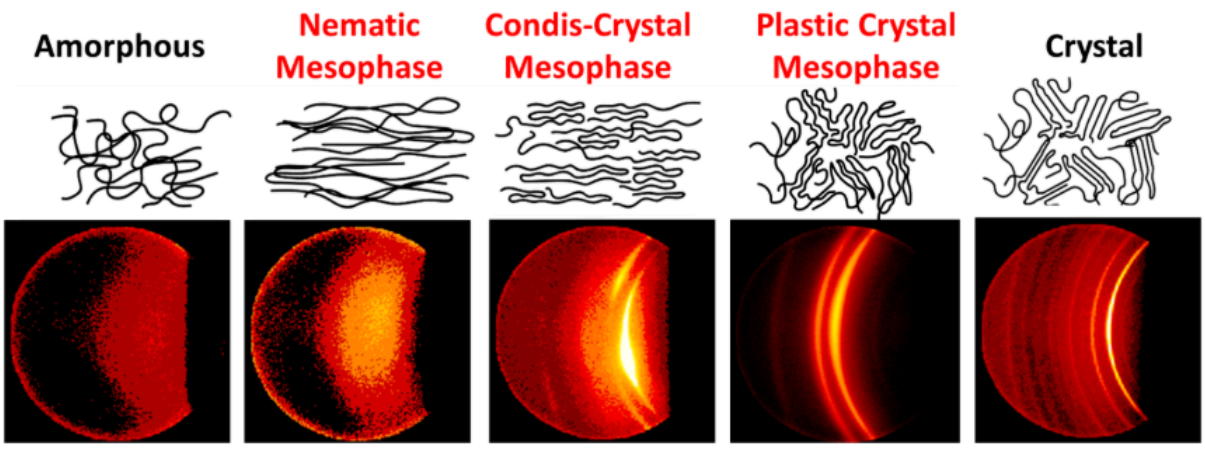

Figure 2: Debye Ring Patterns Associated with Polymer Chain Alignment in Polymer Morphological Phases[29]

The concept of a mesophase describes an intermediate state between amorphous and crystalline structures, characterized by partial ordering that does not fully reach crystalline organization. Mesophases include liquid crystalline, plastic crystalline, and condis crystalline

states (Figure 2), each defined by varying degrees of conformational, positional, and orientational order. While mesophases are not typically inherent to polymer systems, they can be induced through processing conditions such as temperature, pressure, and applied mechanical forces, which promote reorganization of polymer chains.

Previous work in the Mathiowitz laboratory has demonstrated the successful induction of mesophase structures in polymers, including PCL, polylactic acid, and polyethylene glycol under controlled processing conditions [29]. This ability to modulate polymer morphology presents a unique opportunity to influence drug delivery behavior, as intermediate ordering may alter diffusion pathways, polymer packing density, and drug-polymer interactions, ultimately impacting release kinetics and stability.

Polycaprolactone

Poly(ε-caprolactone) (PCL) is a biodegradable, semicrystalline, thermoplastic polymer characterized by a melting temperature of approximately 60 °C and a glass transition temperature (Tg) near −60 °C[30]. Due to its relatively high degree of crystallinity and hydrophobic nature, high molecular weight PCL exhibits slow in vivo degradation kinetics, with degradation times extending up to two years. This degradation occurs primarily through hydrolytic cleavage of ester bonds, followed by enzymatic fragmentation[31].

The physicochemical and mechanical properties of PCL, particularly its degradation behavior, are strongly influenced by intrinsic parameters such as molecular weight and crystallinity[32,33]. These characteristics, combined with its biocompatibility and ease of processing, have led to its widespread use in biomedical applications, particularly in long-term drug delivery systems. As a hydrophobic polymer, PCL is compatible with a wide range of therapeutic agents and is well-suited for sustained release formulations[34].

Recent studies, including those conducted in the Mathiowitz laboratory, have demonstrated the feasibility of inducing mesophase structures within PCL under specific temperature and pressure conditions[29]. Building upon this work, the present study aims to induce mesophase formation in PCL while incorporating rifampicin as a model drug. This approach is designed to investigate how mesophase-induced structural changes influence drug release kinetics and how varying drug loadings impact polymer morphology. By integrating polymer engineering with controlled drug delivery principles, this work seeks to develop a tunable platform for sustained antimicrobial delivery, with potential applications in the treatment of tuberculosis and prosthetic joint infections.

Aims

The following aims guide the objectives of this work:

1. Induce and characterize mesophase in PCL under controlled temperature and pressure conditions, with varying rifampicin loadings.
2. Determine how varying drug loading affects polymer morphology and drug distribution within the polymer-drug matrix.
3. Evaluate how mesophase influences Rifampicin release profiles.

Chapter 2: Materials and Methods

Sample Film Preparation

Film cast samples were created using 250mg of PCL (MW: 37,000, Polysciences Inc.) and Rifampicin (MW: 822.94 g/mol, SigmaAldrich) in varying loading conditions (0%, 1%, 5%, 10%, 15%, 20%, 30%). Once the drug and polymer were weighed, they were dissolved in

dichloromethane in scintillation vials and subjected to 3 rounds of 5 min sonication followed by 1 min vortexing. The solution is then poured into 60 mm petri dishes, the 15%, 20% and 30% loading solutions were poured into aluminum-lined petri dishes and left in the fume hood for 24 hours. Once the DCM is fully evaporated, the resulting films are peeled from the dish/aluminum. For each loading condition, some films were left as is to be used as controls.

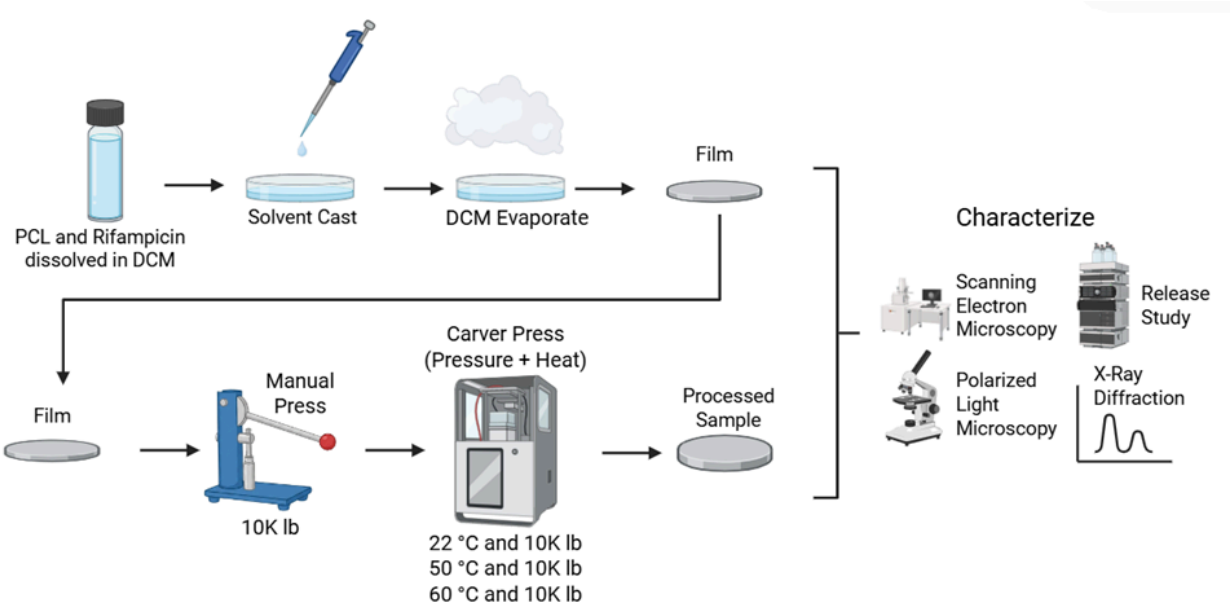

Figure 3: Methods Schematic

After the solvent evaporated (~24 hours), a film cast was formed. The samples were placed into a 13mm diameter cylinder tablet die for the manual press (Specac GS15011 manual hydraulic press) at 10,000 lbs for 5 minutes at room temperature. Subsequently, the newly formed tablets are heat pressed in the Carver Auto Press (Model 2889) between steel plates at temperatures of 22 °C, 50 °C, and 60 °C. The sample is heated to the desired temperature under no pressure for 5 minutes, followed by an active press of 10,000lb for 5 minutes, and then a cooling period while under pressure to 22℃. Each loading condition underwent pressure/heat

processing at the 3 varying parameters, 22℃/10,000 lb, 50℃/10,000 lb, and 60℃/10,000 lb. The samples will be referred to based on their processing temperature and loading in the rest of this work. The overall sample fabrication process is summarized in Figure 3. Ultimately, there are 28 samples from 4 processing parameters and 7 loading conditions. For PLM and XRD analysis, the samples were kept whole and tested as such. In the release studies, 8mm discs were cut from each triplicate and were massed and measured before beginning the release (summarized in *Table 1*)

Table 1: Physical Characteristics of Release Study Samples

			Film 1		Film 2		22C		50C		60C	
% Loading	Triplicate #	Diameter (mm)	Thickness (mm)	Weight (mg)	Thickness (mm)	Weight (mg)	Thickness (mm)	Weight (mg)	Thickness (mm)	Weight (mg)	Thickness (mm)	Weight (mg)
	1	8	0.1	4.0	0.1	3.90	0.8	31.2	0.7	29.49	0.1	4.85
	2	8	0.1	4.0	0.1	3.64	0.7	47.1	0.6	22.6	0.3	15.14
1	3	8	0.1	3.1	0.1	3.94	0.8	47.2	0.6	20.05	0.2	10.59
	1	8	0.1	4.8	0.1	3.80	0.8	50.1	0.7	29.04	0.1	2.46
	2	8	0.1	3.9	0.1	3.80	0.7	42.8	0.8	28.35	0.3	12.22
5	3	8	0.1	3.6	0.1	3.82	0.8	44.6	0.7	26.11	0.3	6.84
	1	8	0.1	4.1	0.1	4.04	0.5	38.4	0.6	29.43	0.1	5.69
	2	8	0.1	3.5	0.1	4.49	0.6	40.8	0.8	31.84	0.2	11.14
10	3	8	0.1	3.2	0.1	3.33	0.8	48.7	0.8	27.62	0.1	7.07
	1	8	0.1	3.5	0.1	8.13	0.6	43.2	0.5	21.25	0.1	7.85
	2	8	0.1	3.2	0.1	5.62	0.9	50.8	0.6	22.29	0.1	7.02
15	3	8	0.1	4.3	0.1	8.82	0.8	45.6	0.5	19.33	0.4	10.14
	1	8	0.1	3.9	0.1	2.97	0.6	44.2	0.5	25.10	0.4	10.15
	2	8	0.1	7.6	0.1	4.46	0.6	46.8	0.6	27.00	0.2	8.15
20	3	8	0.1	4.9	0.1	7.80	0.5	39.8	0.7	31.99	0.4	12.47
	1	8	N/A	N/A	0.1	4.03	N/A	N/A	0.7	27.26	0.4	11.49
	2	8	N/A	N/A	0.1	5.24	N/A	N/A	0.6	23.03	0.2	7.55
30												

	3	8	N/A	N/A	0.1	4.65	N/A	N/A	0.6	23.88	0.1	5.4

Polarized Light Microscopy (PLM)

Polarized Light Microscopy was completed to qualitatively confirm the presence of birefringence and spherulites on a Laxco SeBa Pro4B Series Digital Microscope System with 4x, 10x, 20x, and 40x objectives. Images of prepared samples, both pressure-processed and films, were taken with a 16MP color camera on the SeBa Pro Software.

X-ray Diffraction (XRD)

X-ray diffraction (XRD) was performed using a Bruker D8 X-ray Powder Diffractometer with a Cu X-ray tube operating at 40 kV and 40 mA. A Bruker Vantec500 Xe–CO_2 gas-filled detector with a 13.5 cm diameter window, positioned 20 cm from the goniometer center, was used to collect data. Scans were conducted over a 2θ range of 20° to 80° with a 15° step size, holding each step for 30 seconds. Each scan produced a diffraction spectrum that reflects the material's structural composition based on characteristic peak intensities, along with 2D Debye-Scherrer rings showing the sample's scattering patterns.

XRD Deconvolution

The phase content of samples was calculated from XRD scattering profiles using peak deconvolution in Fityk v.1.3.1. Gaussian profiles were assumed for all peaks, including the broad amorphous halo, which was derived from filmcast PCL and held constant throughout the analysis. Crystalline peaks corresponding to PCL were placed at approximately 2θ = 21°, 22°, and 24° based on literature values [35]. Where necessary, additional mesophase peaks were

included to achieve an optimal fit. All fits were iteratively adjusted to reach an R^2 value of at least 0.99. Phase fractions (crystalline, amorphous, and mesophase) were then calculated from the relative areas under the fitted peaks.

Scanning Electron Microscopy (SEM)

Scanning electron microscopy (SEM) was performed using a Thermo Fisher Scientific Apreo Volume Scope (VS) SEM. Samples were sputtercoated with a gold–palladium layer for 3 minutes at 20 mA using an Emitech K550 sputter coater before imaging. SEM was used to evaluate the distribution of rifampicin within the polymer matrix, visualize internal microstructural features, and assess morphological changes associated with varying drug loadings. The Apreo VS SEM was acquired through a high-end instrumentation grant from the Office of the Director of the National Institutes of Health (S10OD023461).

Release Study

Two in vitro release studies were conducted to evaluate rifampicin release from PCL samples. In both studies, filmcast and pressure-processed PCL discs were prepared as 8 mm samples, preweighed, measured, and submerged in 50 mL of phosphate-buffered saline (PBS) in individual Falcon tubes. At each time point, 15 mL of the release medium was collected at each time point for HPLC analysis, and sink conditions were maintained by removing all old PBS and replacing it with fresh PBS. All sample types, defined by drug loading and processing condition, were prepared and tested in triplicate.

The first study investigated filmcast and pressure processed samples at 22 °C, with rifampicin loadings of 1%, 5%, 10%, 15%, and 20%. Aliquots of 15mL were collected daily during the first week, every other day during the second week, every three days during the third

week, and twice during the fourth week. Of the collected 15mL, a portion was run on the HPLC to quantify rifampicin levels. In the first release study, the samples were run after 6 months of initial collection, which could result in reduced Rifampicin detected via HPLC due to degradation in the PBS.

The second study examined samples processed at 50 °C, 60 °C, and another set of film controls with an expanded set of rifampicin loadings: 1%, 5%, 10%, 15%, 20%, and 30%. During this study, there were weekly collections throughout the study period, where 15mL of PBS was collected from the Falcon tubes, and the remaining medium was discarded and replaced in order to maintain sink conditions. Analysis was done with HPLC immediately after release.

High Performance Liquid Chromatography (HPLC)

Rifampicin detection in the samples from the two drug release studies was performed using a Waters Alliance HPLC System (Milford, Massachusetts), equipped with a Waters 2489 UV/Visible Detector for analysis. An Empower Data System and XTerra column (Waters Corporation) were used for separation and recording the output signal of the detector. The mobile phase was an isocratic mixture of acetonitrile and water (60/40, v/v). The flow rate was 1.0 mL/min, the injection volume was 10 µL, the UV detection wavelength was 475 nm, and the column was maintained at room temperature.

Chapter 3 Results and Discussion:

PLM Images

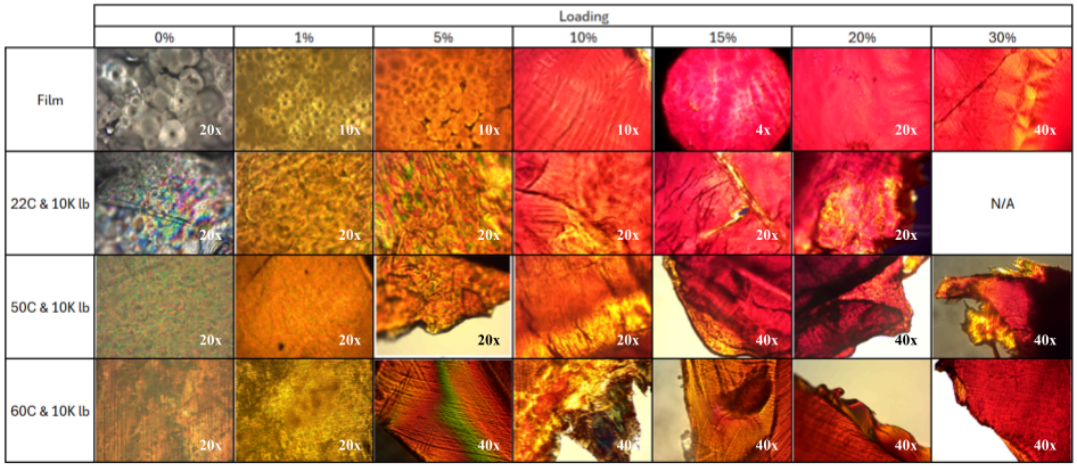

Figure 4: PLM Images

PLM images were acquired for each loading condition across the four processing parameters to qualitatively characterize key features of polymer morphology, specifically, spherulite formation and birefringence. Spherulite formation is clearly visible in filmcast samples at 0%, 1%, and 5% loading (Figure 4), indicating a high degree of crystallinity. In higher-loaded filmcast samples, spherulites are less abundant in comparison. This shows that the drug may have some antagonistic impact on polymer crystallization, resulting in reduced spherulite formation. Upon pressure processing, however, the defined spherulitic structure is absent across all loading conditions. At 22℃, disrupted spherulite structures can be seen in the 0%, 1%, and 5% loadings, with distorted unit cells. The inverse trend is observed for birefringence, where no birefringence is detected in any filmcast samples, yet it emerges in several pressure processed samples. The development of birefringence in pressure-processed samples is indicative of increased molecular alignment and organizational order and serves as a preliminary indicator of pressure induced changes to the internal molecular structure[36]. This effect is most pronounced in

the 0% loading condition, but is also observable at 1% and 5% loading. As with spherulite visualization, increasing rifampicin content progressively obscures the colors emitted from birefrigence, limiting the ability to visually detect birefringence at higher loadings.

PLM gives a qualitative initial understanding of how processing impacts internal polymer morphology, along with the impact of drug loading. Further characterization will provide additional information to further understand the impacts of loading and pressure/temperature processing in a quantitative way.

2D XRD Analysis

All samples underwent XRD analysis to generate Debye-Scherrer rings and XY scattering profiles. As a semicrystalline polymer, PCL typically exhibits two well-defined crystalline peaks with a third smaller peak, corresponding to the (110), (111), and (200) planes of the orthorhombic crystal structure[35]. These are evident in the XY plots as peaks at 2θ values of 21°, 22°, and 24°. In the Debye rings, these crystalline phases manifest as distinct, sharp lines (Figure 5).

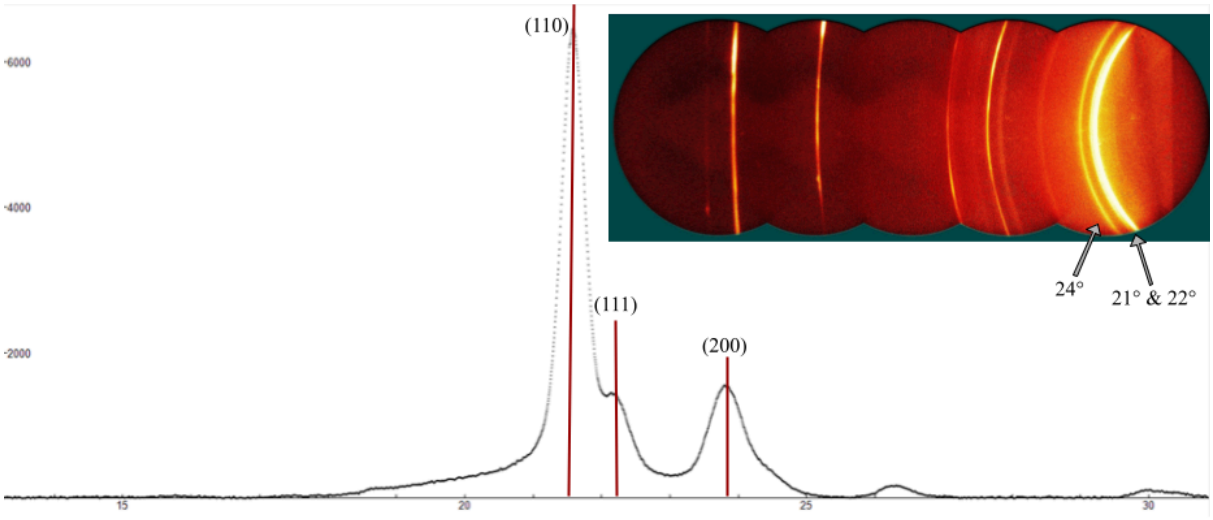

Figure 5: Film PCL XY and Debye Rings

Analyzing the filmcast samples establishes a baseline for understanding how pressure processing alters PCL morphology. Processing at 22°C and 50°C causes the Debye rings to broaden, a trend mirrored by the crystalline peaks in the XY plots (Figure 6). This change in pattern can be attributed to the induction of mesophase. Notably, the peak at 22° corresponding to the (111) plane disappears in these plots. An increase in the broad amorphous region is also observed under the crystalline peaks. Conversely, samples processed at 60°C maintain prominent peak shapes and intensities as seen in the film cast. However, the base of these peaks is wider, and the amorphous region is larger. The broad diffusion in the Debye rings surrounding the crystalline rings at 60°C suggests the presence of a mesophase.

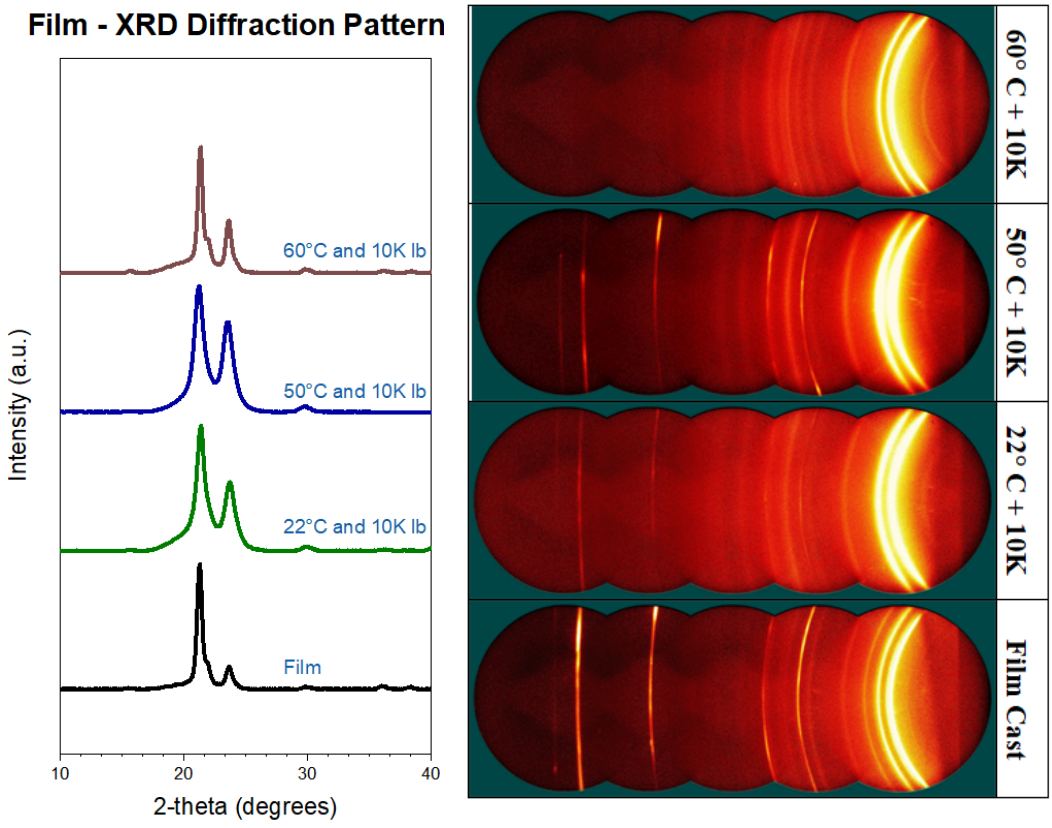

Figure 6: Pure PCL a. XY Plots and b. XRD Debye Rings Across Processing Parameters

Processing parameters were selected based on previous Mathiowitz Lab research, which identified conditions favoring specific mesophase types, namely condis crystal and plastic crystal. These are identifiable via distinct Debye patterns[29].

At 22°C, the Debye rings thicken along with the peak profiles, indicative of a decrease in crystallite size or an increase in structural disorder. Since samples were processed below PCL's melting temperature, the applied pressure likely induces plastic deformation, disrupting the initial orthorhombic crystal structure. Plastic crystal mesophases are characterized by positional order with conformational and orientational disorder, and the broadened isotropic crystalline peaks observed in XRD are consistent with this type of mesophase formation.

At 50°C, near the onset of PCL's melting temperature, the Debye rings display an anisotropic arc concentrated around the equator, reflecting positional order with conformational disorder. This equatorial focus arises from the orientation of polymer chains in the radial direction, normal to the axis of compression. A change in the (111):(200) peak ratio relative to the film cast sample is also observed, further supporting the formation of a condis crystal mesophase characterized by positional and orientational order with conformational disorder [37].

In the pure PCL samples processed at 60°C, the scattering pattern closely resembles that of the film cast samples, with sharp crystalline peaks and Debye rings reflecting high crystallinity. A slight broadening of the crystalline peak bases is observed alongside an increase in the amorphous area, suggesting a modestly less ordered structure. This is contrary to the findings of Baptista et al., where processing at 60°C produced results similar to those at 50°C. The key difference between the two studies is in sample preparation; samples in this work were film cast, whereas those in Baptista's work were melt processed. Film casting is known to produce lower degrees of crystallinity and depressed melting temperatures relative to melt cast

samples [38], suggesting that the film cast samples in this study were above their effective melting temperature at 60°C. This results in a more semicrystalline morphology rather than the condis crystal mesophase observed by Baptista et al.

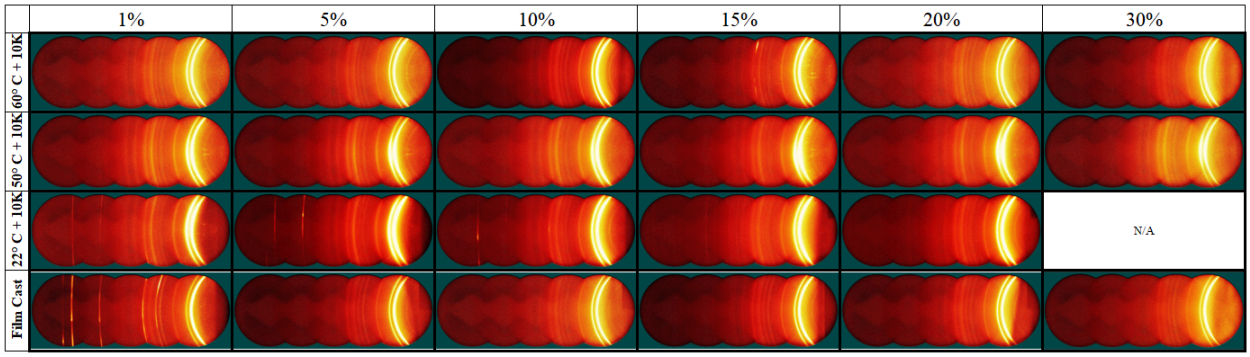

Figure 7: Debye Rings of Loaded Samples Across Processing Parameters

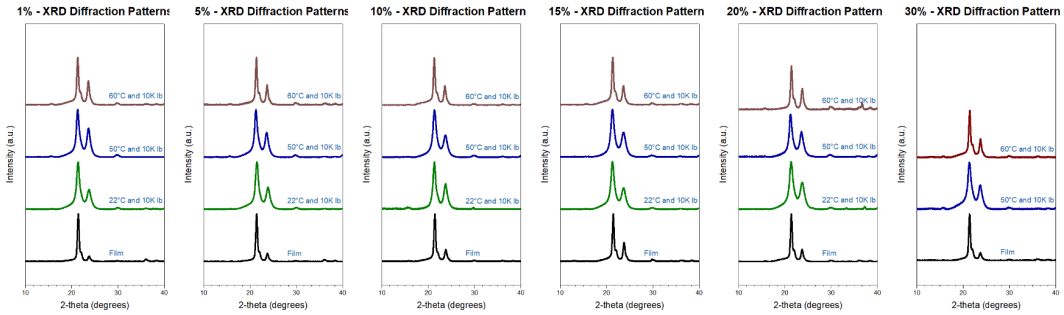

Figure 8: XY Plots over Loading and Pressure Processing

The loaded samples all show similar patterns to those of the pure PCL sample, with an interesting phenomenon where the drug crystal peaks never become apparent, as seen in Figure 8, where even at 30% loading, the peaks never protrude heavily from the PCL scattering profile or in the Debye rings (Figure 7). It is also evident in the Debye rings that the patterns from the pure PCL samples hold. The 22°C samples have isotropic broadening of the rings, while the 50°C samples have broadening focused near the equator. Similarly, at 60°C, there is recrystallization indicated by the sharp lines. The XY plots also have the same pattern as pure

PCL, with broadening of the crystalline peaks at 50°C and 22°C, and an increase in the amorphous regions and the emergence of crystalline peaks at 60 °C. This indicates that mesophase induction remains consistent with what is seen in pure PCL, as the varying processing parameters are first looked at in this qualitative data.

Deconvolution

Peak fitting of the XRD data confirms quantitatively that pressure processing induces mesophase formation across all loading levels, which is consistent with what was observed in the PLM and Debye ring analysis. The same overall trend seen in the 0% samples (Figure 9) carries through to the loaded systems, and this is more clearly visualized in Figure 10.

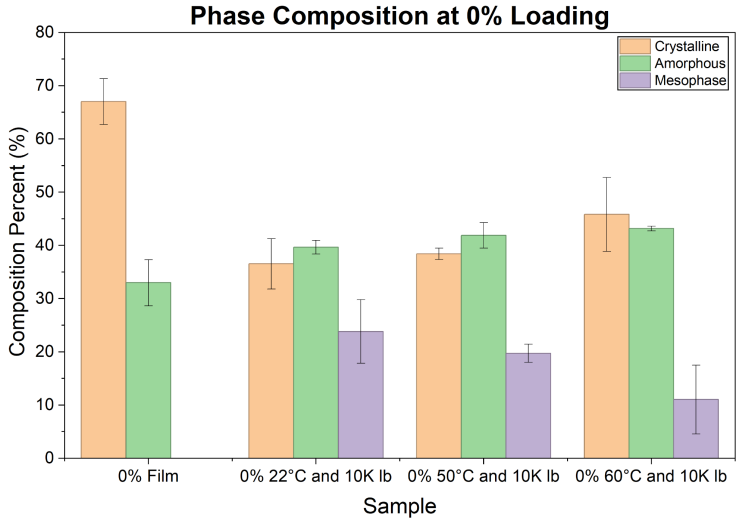

Figure 9: Phase Composition at 0% Loading

Analyzing the 0% loaded samples, it can be seen that filmcast samples are predominantly crystalline, with crystallinity values consistently ranging from approximately 60–70% and minimal to no detectable mesophase content (0–6%). This is expected given the absence of any applied mechanical stimulus capable of disrupting the native orthorhombic structure. Notably, at

higher drug loadings (≥10%), a modest but reproducible increase in mesophase content (up to ~5–6%) is observed, suggesting that elevated Rifampicin concentrations begin to interfere with polymer chain packing to generate lyotropic mesophase.

For the loaded samples, it can be seen that a similar overall trend remains true, whereupon introduction of pressure, a pronounced and reproducible shift in phase composition is observed. Mesophase content increases substantially to 20–35% across the majority of samples, while crystallinity correspondingly decreases to the 25–38% range. This trend is consistent across loading conditions and supports the interpretation that compression disrupts existing crystalline domains and drives the system toward intermediate mesophase organization. Processing at 50 °C yields some of the highest observed mesophase fractions (up to ~36–37%), consistent with a processing window in which thermal energy imparts sufficient chain mobility for structural reorganization without permitting full relaxation into stable crystalline structures.

At 60 °C, the phase composition shifts back toward greater crystallinity (~45–58%), with a corresponding reduction in mesophase content. This behavior is consistent with 60 °C falling within the effective melting range of filmcast PCL (55–65 °C), where elevated chain mobility enables reorganization into thermodynamically stable crystalline structures during the pressurization and cooling cycle.

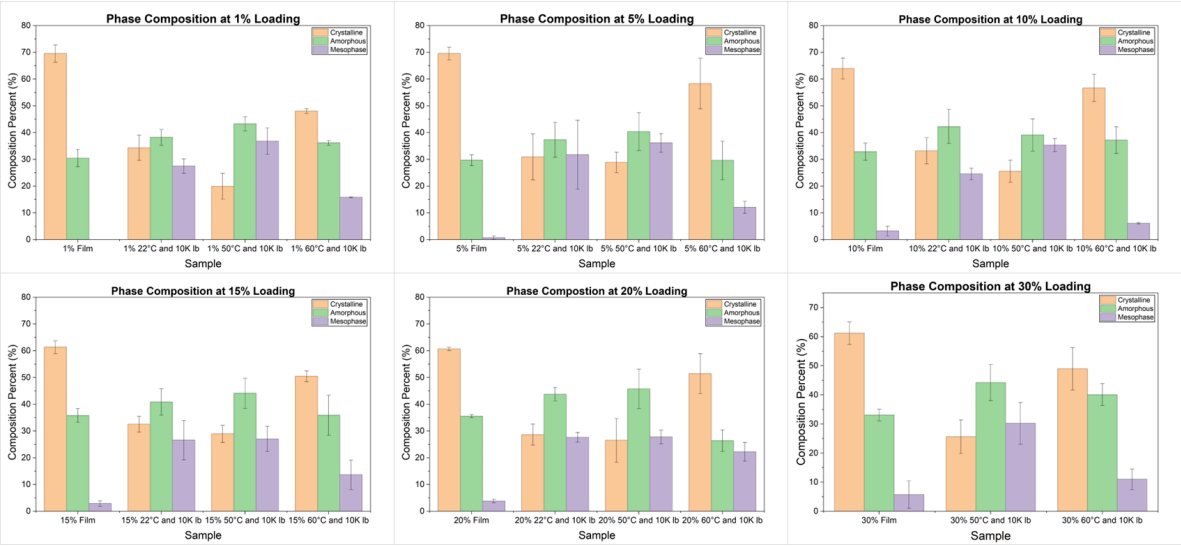

Figure 10: Morphological Phase Calculations of Samples Grouped Based on Loading Percent

Across all processing conditions, the amorphous fraction remains comparatively stable (~30–45%), indicating that the principal structural transition occurs between crystalline and mesophase domains rather than toward a global increase in disorder. Taken together, these results establish processing temperature as the primary determinant of polymer morphology, where pressure processing at temperatures below the melt point (22–50 °C) favors high levels of mesophase induction, while processing at 60 °C drives the system back toward semicrystalline organization. These conclusions align with the qualitative observations from PLM, Debye ring, and XY scattering analyses.

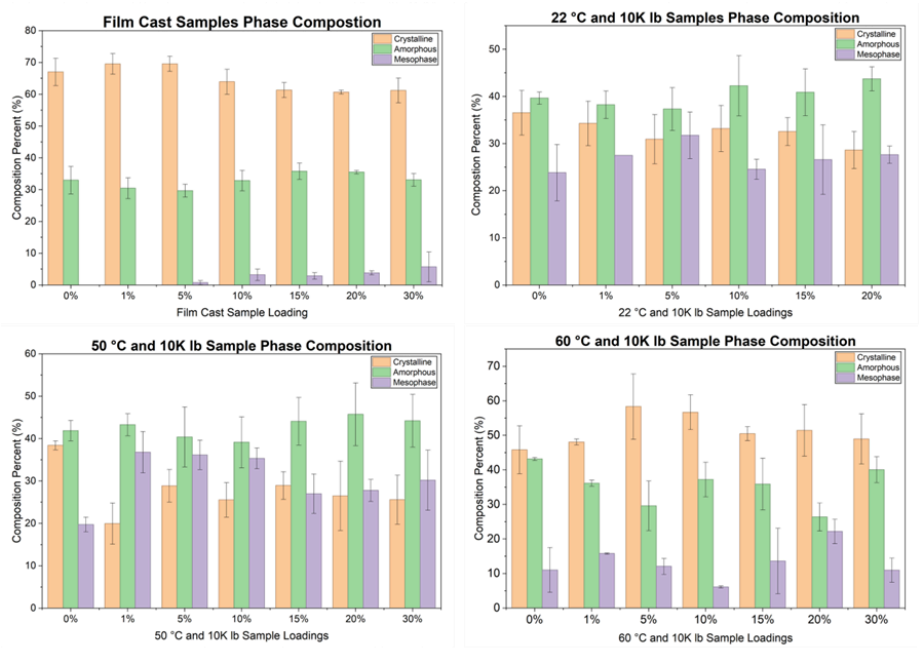

Figure 11: Morphological Phase Calculations of Samples Grouped Based on Processing

A two-way ANOVA was performed on the deconvolution data to determine how processing conditions and drug loading influence mesophase formation. Processing had a highly significant effect ($F(3,54) = 107.5$, $p < 0.0001$), showing that changes in processing conditions strongly drive differences in mesophase content. In comparison, loading had a smaller but still statistically significant effect ($F(6,54) = 2.38$, $p = 0.041$), suggesting only a minor contribution. The interaction between processing and loading was not significant ($F(18,54) = 1.74$, $p = 0.061$), indicating that the effect of processing is consistent across different loading levels. Tukey post hoc analysis showed significant differences between most processing groups, except for the 22 °C and 50 °C conditions, which were not significantly different from each other. No significant differences were observed between loading fractions. Overall, these results show that processing

is the main factor controlling mesophase formation, while loading has a much smaller and less meaningful effect.

Scanning Electron Microscopy

Filmcast samples were analyzed using SEM to further characterize their surface and internal morphology and to support the observed release profiles. Surface images showed no visible drug across all loading levels, suggesting that rifampicin is fully dispersed within the polymer matrix in a minimally crystalline state. Spherulitic structures were evident up to 15% loading (Figure 12). At this concentration, a distinct fingerprint-like pattern with concentric rings appeared within the spherulites. However, at 20% and 30% loadings, spherulites were no longer observed on the surface, consistent with PLM results indicating that higher rifampicin content can disrupt polymer crystallinity.

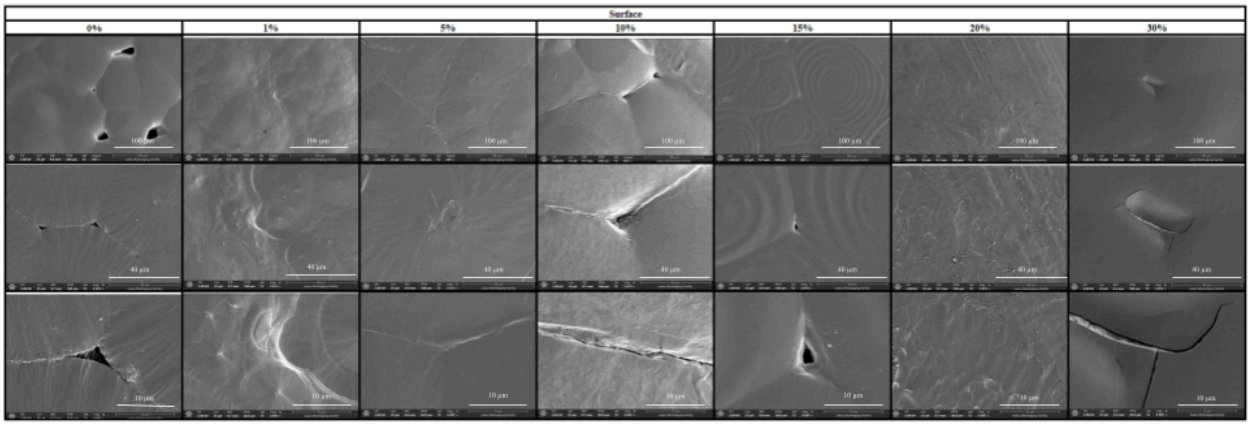

Figure 12: Surface SEM Images

Cross-sectional imaging revealed that at lower drug loadings, no distinct rifampicin crystals extended beyond the PCL matrix. Only small, irregular “bumpy” regions were observed,

which may represent early-stage drug aggregation or the onset of crystallization. At 20% loading, discrete crystalline structures began to emerge from the matrix, as circular features within the PCL. These crystals became more prominent and abundant at 30% loading, along with a noticeable increase in polymer porosity (Figure 12). These findings are consistent with the XRD results, where rifampicin-specific peaks were not observed to dominate or clearly emerge over the PCL peaks even at higher loadings. Ultimately, this indicates that the drug remained largely amorphous or insufficiently crystalline and was well-embedded within the polymer matrix, making it difficult to be distinctly detected. To this end, it would be expected that the drug release amounts will be proportional to its loading.

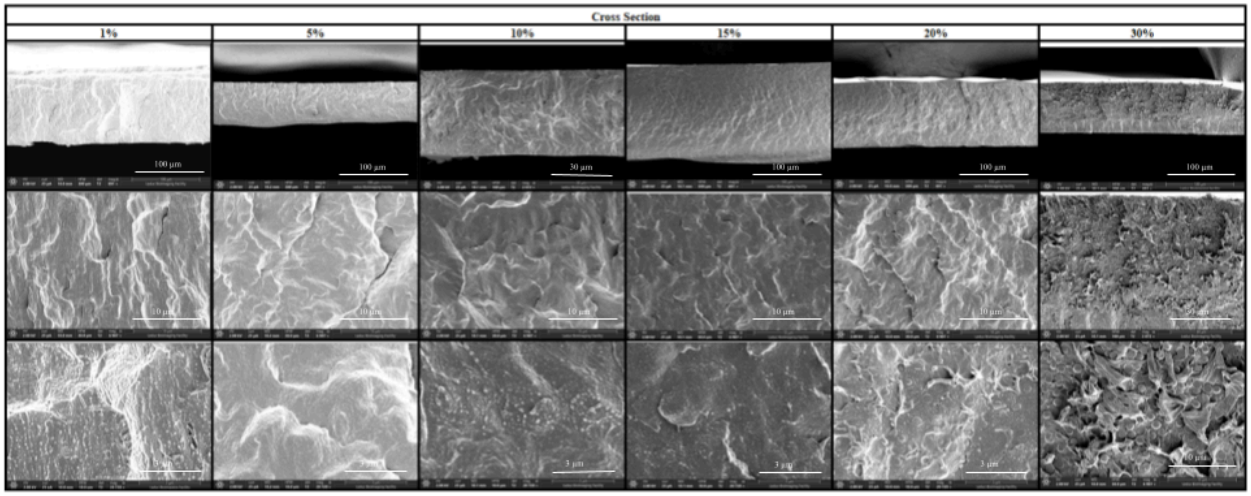

Figure 13: Cross-Section SEM Images

Release Study

First Release Study (Film vs. Processing at 22℃ and 10,000 lb)

The release profiles from Study 1 were analyzed to evaluate how drug loading and processing conditions influence total drug release and release kinetics over the 28-day study window.

Figure 14a presents total cumulative drug release and reveals a clear positive correlation between drug loading and total release across both processing conditions, a trend consistent across all formulations. The 20% film formulation reaches ~87.96 µg total release by day 28, while lower loadings such as 10% and 5% plateau at ~47.59 µg and ~26.97 µg, respectively. For the processed sample, the 15% loaded sample released the most drug at ~155.33 µg while the 1% sample released ~22.37 µg.

Notably, filmcast samples exhibit a pronounced burst phase followed by an early plateau, typically reached by approximately day 5, indicating rapid drug depletion from the matrix. In contrast, pressure processed samples sustain a more gradual, continuous release throughout the full experimental period. This distinction is further clarified in Figure 14b, which normalizes release as a percentage of the total drug content theoretically loaded in the samples. filmcast samples consistently achieve higher early percent release before plateauing sharply, while pressure processed samples maintain comparatively lower but steadily increasing percent release values across the study duration, indicative of a more controlled and sustained release mechanism

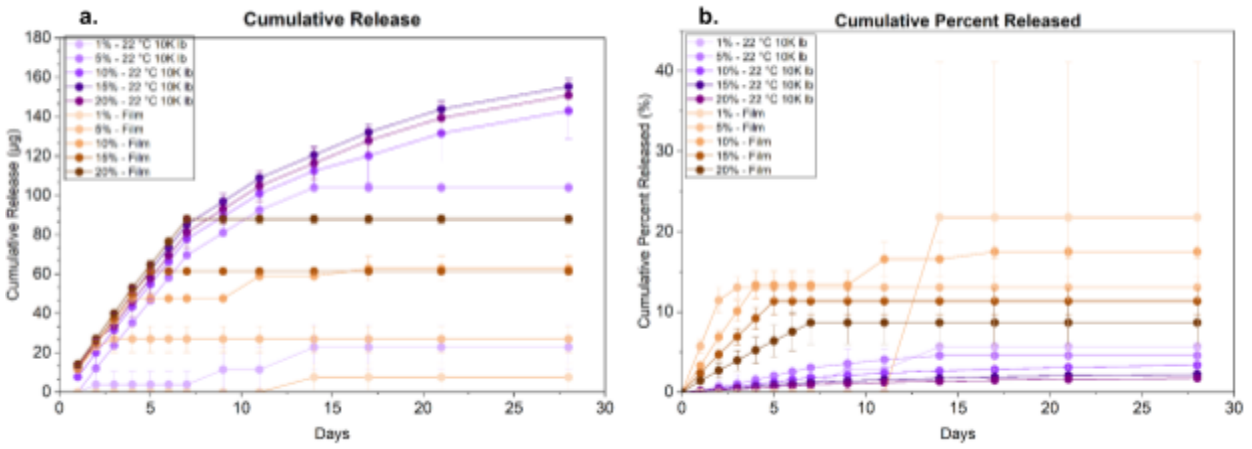

Figure 14: Cumulative Percent and Total Releases of Rifampicin from Release Study 1

Figure 15 reinforces these observations by separating the percent release according to drug loading. filmcast formulations release a disproportionately large fraction of their drug content early, followed by a rapid plateau, whereas pressure-processed formulations exhibit a near-linear, gradual increase over time. It appears that the pressure processed formulations had not yet reached a plateau by day 28, suggesting that release remained ongoing and may extend beyond the study window.

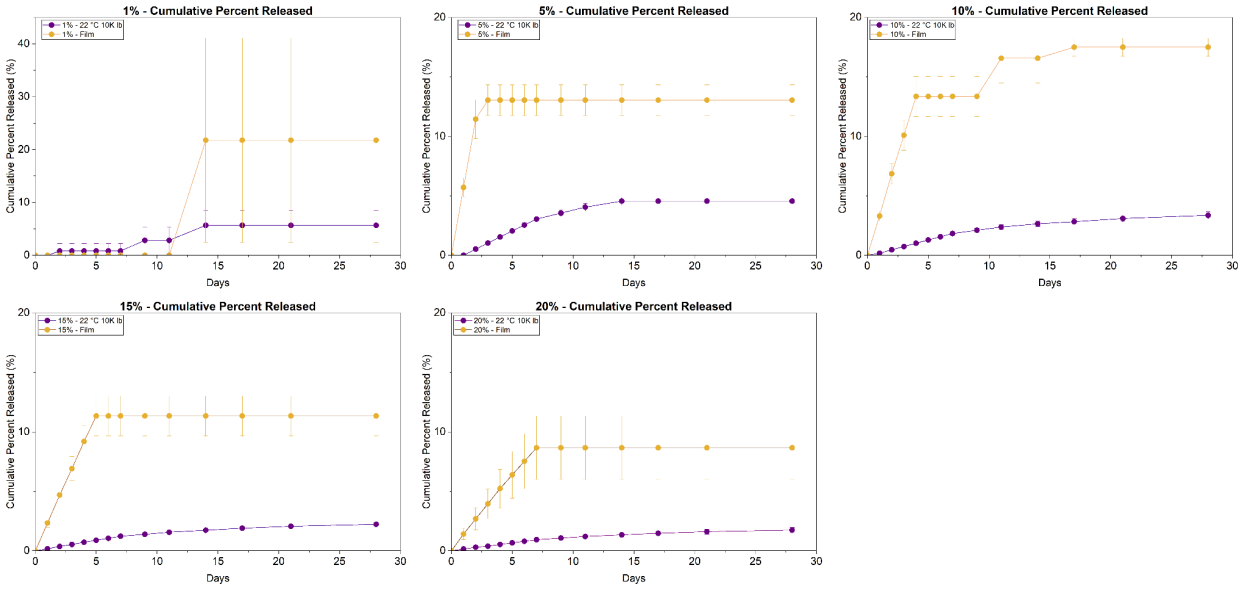

Figure 15: Cumulative Release Percent Graphs Separated by Loading

An important consideration in this study is that although the samples were subjected to the in vitro release protocol as fresh materials, the collected PBS samples were stored for a period of time before HPLC analysis. Rifampicin is known to degrade in aqueous environments such as PBS through nonenzymatic autooxidation to rifampicin quinone, which may result in an underestimation of release values since the HPLC method detects only the parent compound[39].

Release Study 2 (Film vs Processing at 50℃ and 10,000 lb vs 60℃ and 10,000 lb)

The second release study examined the influence of processing temperature on drug release behavior, comparing formulations processed at 50°C and 60°C under identical pressure conditions against filmcast controls. As shown in Figure 16, cumulative drug release scales with drug loading across all processing groups, consistent with the homogeneous dispersion of rifampicin within the PCL matrix observed in Study 1 and seen in SEM images. When release is normalized as a percent of total drug content, however, clear stratification by processing condition emerges. Filmcast samples occupy the uppermost band of the release profile (orange), reflecting rapid early burst release and swift matrix depletion. The 60°C pressure processed samples fall below the films (blue), while the 50°C pressure processed (teal) samples display the lowest percent release values throughout, indicating the most sustained and controlled release behavior of the three groups.

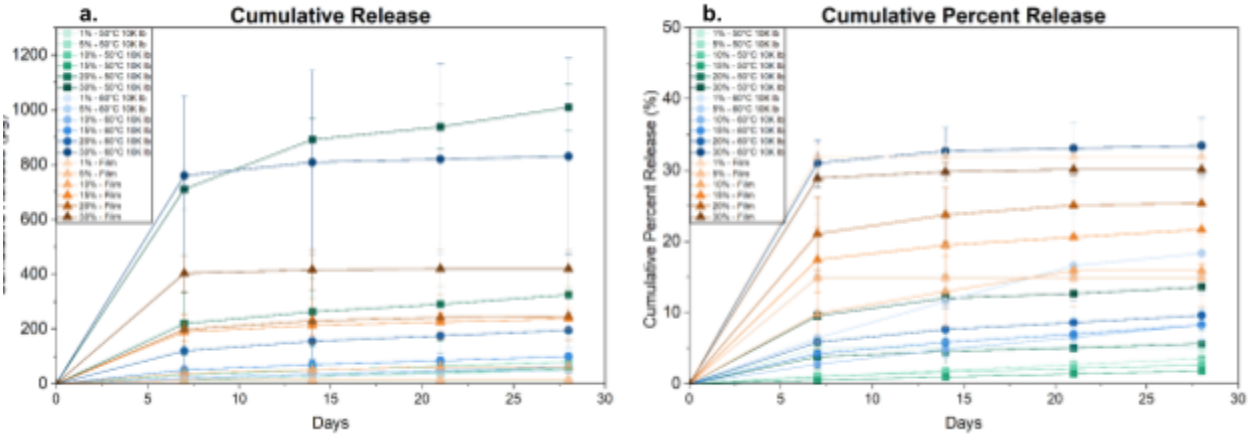

Figure 16: Cumulative Percent and Total Releases of Rifampicin from Release Study 2

Separation by drug loading further highlights the influence of processing conditions on rifampicin release behavior (Figure 17). The 50 °C processed samples consistently exhibited slower, more gradual rifampicin release compared to both the 60 °C processed and film-cast

groups. Additionally, the processed samples demonstrated a more linear and sustained release profile, whereas the film-cast samples released drug rapidly during the initial period before reaching a plateau.

The differences observed between the processed sample groups further suggest that factors beyond mechanical compression alone are contributing to release kinetics. Although the 50 °C and 60 °C samples underwent the same pressure treatment, the 60 °C samples released rifampicin at a faster rate. These release trends correlate with differences in mesophase content, as the 50 °C samples exhibited the highest mesophase content alongside the slowest release behavior. This relationship indicates that internal polymer morphology and mesophase organization play a significant role in governing drug diffusion and release kinetics, rather than mechanical compression alone.

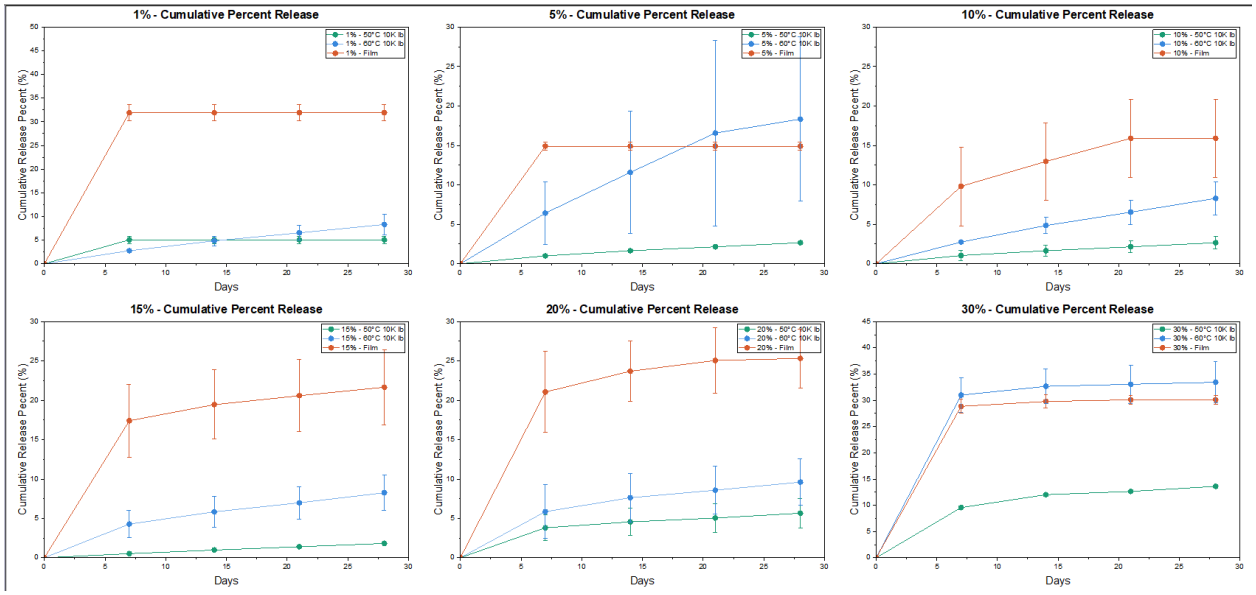

Figure 17: Cumulative Release Percent Graphs Separated by Loading

Taken together, the findings from Release Study 2 reinforce and extend those of Study 1. Across both studies, a consistent pattern emerges: filmcast systems are dominated by rapid

release and early drug depletion, while pressure processed mesophase induced systems retain drug within the polymer and are capable of sustaining release well beyond the 28 day experimental window. The temperature dependence observed in Study 2 further implicates polymer morphology as the primary determinant of release kinetics, offering a mechanistic basis for optimizing controlled delivery performance through processing condition selection.

Correlating Mesophase and Release

To quantify the relationship between polymer structure and release behavior, a correlation analysis was performed between percent mesophase content and cumulative drug release at 28 days. A statistically significant negative correlation was observed ($r = -0.786$, $R^2 = 0.681$, $p < 0.0001$, $n = 16$), demonstrating that increasing mesophase content is associated with reduced drug release (Figure 18a). To account for potential variability introduced by delayed HPLC analysis in the initial dataset, a secondary analysis excluding this dataset was performed. The negative correlation remained robust ($r = -0.796$, $R^2 = 0.633$, $p < 0.001$, $n = 16$) (Figure 18b). In this refined analysis, each 1% increase in mesophase corresponded to an approximate 0.57% decrease in cumulative release. One sample was excluded due to delayed assay timing, and a further outlier was removed to improve statistical consistency.

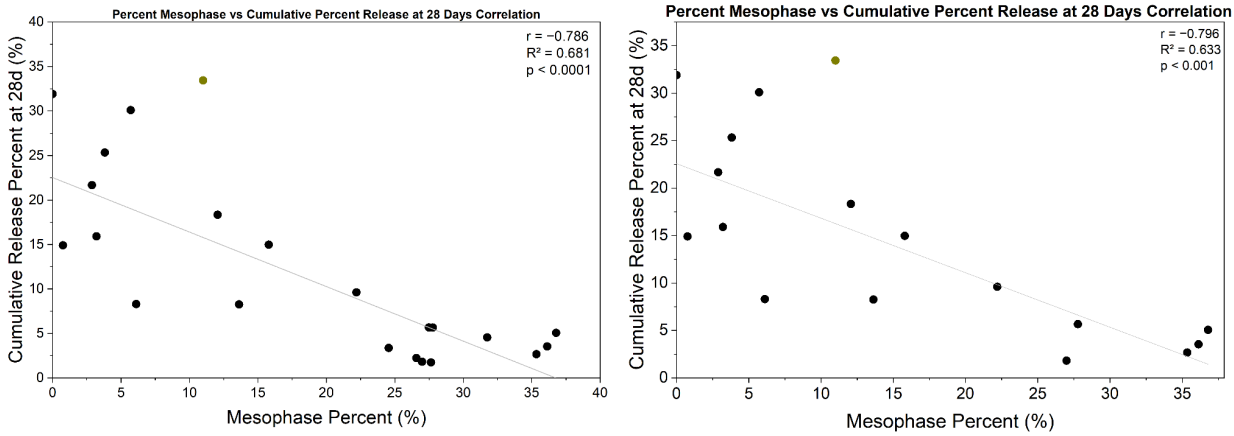

Figure 18: Percent Mesophase and Cumulative Percent Release at 28 Day Correlation

Chapter 4: Conclusions and Future Directions

This study investigated the relationship between polymer morphology, drug loading, and drug release using polycaprolactone (PCL) and rifampicin. Specifically, the feasibility of inducing a mesophase within PCLrifampicin matrices was explored, alongside an examination of how PCL's morphological state influences drug delivery behavior. Through PLM, XRD, and SEM, the morphology and structure of PCL matrices were characterized across a range of rifampicin loadings (1%, 5%, 10%, 15%, 20%, and 30%).

PLM revealed increasing birefringence with pressure processing at 22°C, 50°C, and 60°C, reflecting greater internal chain alignment and order [44,] and serving as a preliminary indicator of mesophase formation. Analysis of the Debye–Scherrer rings revealed that processing at 22°C and 50°C resulted in the diffusion of the crystalline rings, whereas processing at 60°C yielded sharper reflections against a more diffuse background. Together, the changes in the Debye ring profiles and 2D azimuthal XRD patterns allowed for discrimination between the types of mesophase induced, consistent with patterns previously reported in the Mathiowitz lab by Baptista et al. These patterns are consistent in the pure PCL and loaded samples, indicating that mesophase can still be induced in loaded samples, and patterns remain consistent in pure

PCL. SEM provided further insight into how cross-sectional and surface morphology evolve with increasing rifampicin content. Notably, the absence of visible drug crystals was observed up to a 15% loading, and the disruption of the spherulite structure occurred at 20% and 30% loadings, suggesting that higher drug concentrations begin to interfere with PCL's ability to organize.

Drug release studies demonstrated that pressure processing at 22°C and 50°C produced more consistent, prolonged, and slower rifampicin release compared to filmcast controls and 60°C. Taken together, the two release studies reveal a statistically significant inverse correlation between mesophase content and cumulative percent drug released at study endpoint. Critically, the divergence in release behavior between the 22°C/50°C (high mesophase) and 60°C (low mesophase) conditions demonstrates that differences in release kinetics are attributable to changes in internal polymer morphology rather than to the mechanical effects of pressure processing alone. Collectively, this work represents another system demonstrating the impact of mesophase induction on sustained release and the potential of precise polymer processing to control drug delivery outcomes.

This system, as designed, has limited clinical relevance because Rifampicin is not used as monotherapy in either prosthetic joint infections (PJI) or tuberculosis (TB). Moreover, the high systemic dosing required for TB (600 mg/day) makes a long-term implant approach impractical; achieving a 30-day release at 30% drug loading would necessitate an approximately 57 g device, which is not feasible. In contrast, a localized delivery strategy is more suitable for PJI, where the biofilm minimum bactericidal concentration (MBC) for *S. aureus* (0.1–1 μg/mL) supports a target release rate of approximately 200–300 μg/day[47]. At 30% loading, this corresponds to a much more practical ~15 mg PCL–Rifampicin implant for a 14-day treatment period. Although

incorporating combination therapy would improve clinical relevance, these findings still highlight the potential of mesophase-based systems to enable sustained, long-term drug delivery.

Ongoing work aims to characterize the drug release profiles of both processed and filmcast systems beyond the four-week window examined here. Given rifampicin's antimicrobial properties, future antimicrobial testing would help confirm drug efficacy within the PCL matrix and establish how long these systems remain therapeutically active. For delivery applications, properly shaped PCL-Rifampicin matrices should be characterized, as surface geometry is known to influence release kinetics. Additionally, incorporating rifampicin alongside isoniazid or pyrazinamide within the PCL matrix would also move this system toward greater clinical relevance, as TB is treated with a combination therapy approach[44.] For periprosthetic joint infection applications, the mechanical properties of PCLrifampicin films should be studied, given the additional wear requirements for an implant coating. Another area of interest would be the incorporation of rifampicin into high-density polyethylene, which is already widely used in orthopedic implants and spacers[46].

In summary, polymer engineering represents a powerful and versatile tool in drug delivery, and this study further demonstrates that mesophase induction through temperature and pressure processing is a meaningful tool for tailoring polymeric behavior and, by extension, system-level performance. The results also highlight the importance of accounting for polymer-drug interactions during the design phase of drug delivery systems, as these interactions have clear consequences for morphology and release. This work contributes to a growing body of evidence supporting the utility of mesophase engineering in biodegradable polymer systems and their application to controlled drug delivery.

References

1. Agrawal S, et al. Solid state characterization of rifampicin samples and its biopharmaceutic relevance. Eur J Pharm Sci. 2004;22(23):127–144.
2. Wehrli W. Rifampin: mechanisms of action and resistance. Rev Infect Dis. 1983;5(Suppl 3):S407–S411.
3. Abulfathi AA, et al. Clinical pharmacokinetics and pharmacodynamics of rifampicin in human tuberculosis. Clin Pharmacokinet. 2019;58(9):1103–1129.
4. Wells WA, et al. Size and usage patterns of private TB drug markets in the high-burden countries. PLoS One. 2011;6(5):e18964.
5. Niemi M, et al. Pharmacokinetic interactions with rifampicin: clinical relevance. Clin Pharmacokinet. 2003;42(9):819–850.
6. Zaw MT, Emran NA, Lin Z. Mutations inside the rifampicin resistance-determining region of the rpoB gene associated with rifampicin resistance in Mycobacterium tuberculosis. J Infect Public Health. 2018;11(5):605–610.
7. Widmer AF, et al. Antimicrobial treatment of orthopedic implant-related infections with rifampin combinations. Clin Infect Dis. 1992;14(6):1251–1253.
8. Acocella G. Clinical pharmacokinetics of rifampicin. Clin Pharmacokinet. 1978;3(2):108–127.
9. Hussain A, et al. Novel approach for transdermal delivery of rifampicin using a cationic nanoemulsion gel. Int J Nanomedicine. 2020;15:1073–1094.
10. Zimmerli W, et al. Role of rifampin for treatment of orthopedic implant-related staphylococcal infections: a randomized controlled trial. JAMA. 1998;279(19):1537–1541.
11. Vargason AM, Anselmo AC, Mitragotri S. The evolution of commercial drug delivery technologies. Nat Biomed Eng. 2021;5(9):951–967.
12. Alqahtani MS, et al. Advances in oral drug delivery. Front Pharmacol. 2021;12:618411.
13. Sahoo D, et al. Oral drug delivery of nanomedicine. In: Theory and Applications of Non-Parenteral Nanomedicines. Academic Press; 2021:181–207.
14. Stoner KL, et al. Intravenous versus subcutaneous drug administration: which do patients prefer? A systematic review. Patient. 2014.
15. Zhao L, et al. Topical drug delivery strategies for enhancing drug effectiveness by skin barriers, drug delivery systems and individualized dosing. Front Pharmacol. 2024;14:1333986.
16. Adepu S, Ramakrishna S. Controlled drug delivery systems: current status and future directions. Molecules. 2021;26(19):5905.

17. Ezike TC, et al. Advances in drug delivery systems, challenges and future directions. Heliyon. 2023;9(6):e17488.
18. Patel P, Rosani A. Rifampin. In: StatPearls [Internet]. Treasure Island (FL): StatPearls Publishing; 2026.
19. Hiremath SP, Saha RN. Design and study of rifampicin oral controlled release formulations. Drug Deliv. 2004;11(5):311–317.
20. Dartois V. The path of antituberculosis drugs: from blood to lesions to mycobacterial cells. Nat Rev Microbiol. 2014;12(3):159–167.
21. Huanbutta K, et al. Rise of implantable drugs: a chronicle of breakthroughs in drug delivery systems. Saudi Pharm J. 2024;32(12):102193.
22. Namazi H. Polymers in our daily life. BioImpacts. 2017;7(2):73–74.
23. Jiang M, et al. Latest advancements and trends in biomedical polymers for disease prevention, diagnosis, treatment, and clinical application. J Control Release. 2025;380:138–174.
24. Kurowiak J, et al. Biodegradable polymers in biomedical applications: a review. Int J Mol Sci. 2023;24(23):16952.
25. Idrees H, et al. A review of biodegradable natural polymer based nanoparticles for drug delivery applications. Nanomaterials. 2020;10(10):1970.
26. Liechty WB, et al. Polymers for drug delivery systems. Annu Rev Chem Biomol Eng. 2010;1:149–173.
27. Roy D, et al. Rheology of crystallizing polymers: the role of spherulitic superstructures, gap height, and nucleation densities. J Rheol. 2019;63(6).
28. shi NQ, et al. Impact of amorphous and semicrystalline polymers on the dissolution and crystallization inhibition of pioglitazone solid dispersions. Powder Technol. 2013;247:211–221.
29. Baptista C, et al. The effect of temperature and pressure on polycaprolactone morphology. Polymer. 2020;191:122227.
30. Harrison KL, Jenkins MJ. The effect of crystallinity and water absorption on the dynamic mechanical relaxation behaviour of polycaprolactone. Polym Int. 2004;53(9):1298–1304.
31. Sun H, et al. The in vivo degradation, absorption and excretion of PCLbased implant. Biomaterials. 2006;27(9):1735–1740.
32. Woodward SC, et al. The intracellular degradation of poly(εcaprolactone). J Biomed Mater Res. 1985;19(4):437–444.
33. McEachin Z, Lozano K. Production and characterization of polycaprolactone nanofibers via forcespinning technology. J Appl Polym Sci. 2012;126(2):473–479.

34. Woodruff MA, Hutmacher DW. The return of a forgotten polymer—polycaprolactone in the 21st century. Prog Polym Sci. 2010;35(10):1217–1256.

35. Peng H, et al. Morphology and thermal degradation behavior of highly exfoliated CoAllayered double hydroxide/polycaprolactone nanocomposites. Thermochim Acta. 2010;502(12):1–7.

36. Zoetelief WF, Douven LFA, Ingen Housz AJ. Residual thermal stresses in injection molded products. Polym Eng Sci. 1996;36(14):1886–1896.

37. Wunderlich B. A classification of molecules, phases, and transitions as recognized by thermal analysis. Thermochim Acta. 1999;340:37–52.

38. Ranakoti L, et al. Critical review on polylactic acid: properties, structure, processing, biocomposites, and nanocomposites. Materials. 2022;15(12):4312.

39. Phogole CM, et al. In vitro optimization of crushed drugsensitive antituberculosis medication when administered via a nasogastric tube. Microbiol Spectr. 2024;12(1):e0287623.

40. Tuli SM. General principles of osteoarticular tuberculosis. Clin Orthop Relat Res. 2002;(398):11–19.

41. EUCAST. Clinical breakpoints — Mycobacterium tuberculosis. Version 13.0; 2023.

42. Bauer S, et al. Pharmacokinetics of intraarticular drug clearance. J Pharmacokinet Pharmacodyn. 2011;38:355–373.

43. Larsen K, et al. Postsurgical knee joint fluid volume reference. 2014.

44. Geary JM, et al. The mechanism of polymer alignment of liquid crystal materials. J Appl Phys. 1987;62(10):4100–4108.

45. Pouplin T, et al. Isoniazid, pyrazinamide and rifampicin content variation in split fixed dose combination tablets. PLoS One. 2014;9(7):e102047.

46. Lekkala S, et al. Antibiotic-loaded ultrahigh molecular weight polyethylenes. Macromol Biosci. 2024;24(4):2300389.

47. Qayoom, Irfan et al. “Local and Sustained Delivery of Rifampicin from a Bioactive Ceramic Carrier Treats Bone Infection in Rat Tibia.” ACS infectious diseases vol. 6,11 (2020): 2938-2949. doi:10.1021/acsinfecdis.0c00369

Appendix

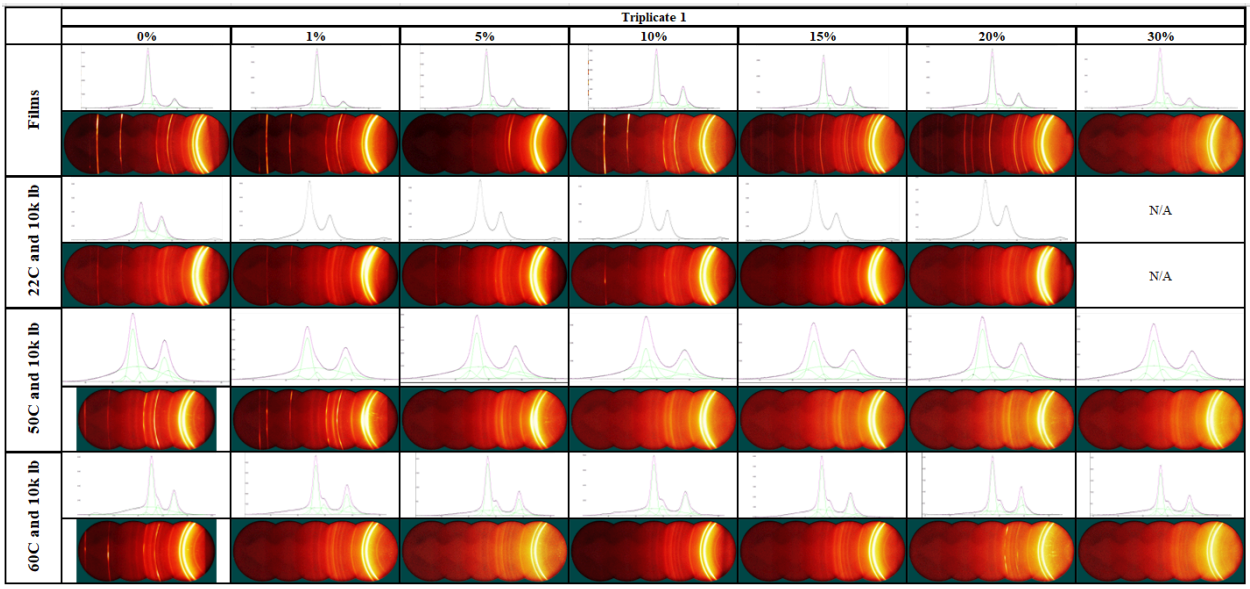

Triplicate 1 - Debye Ring and XY Scattering Plots

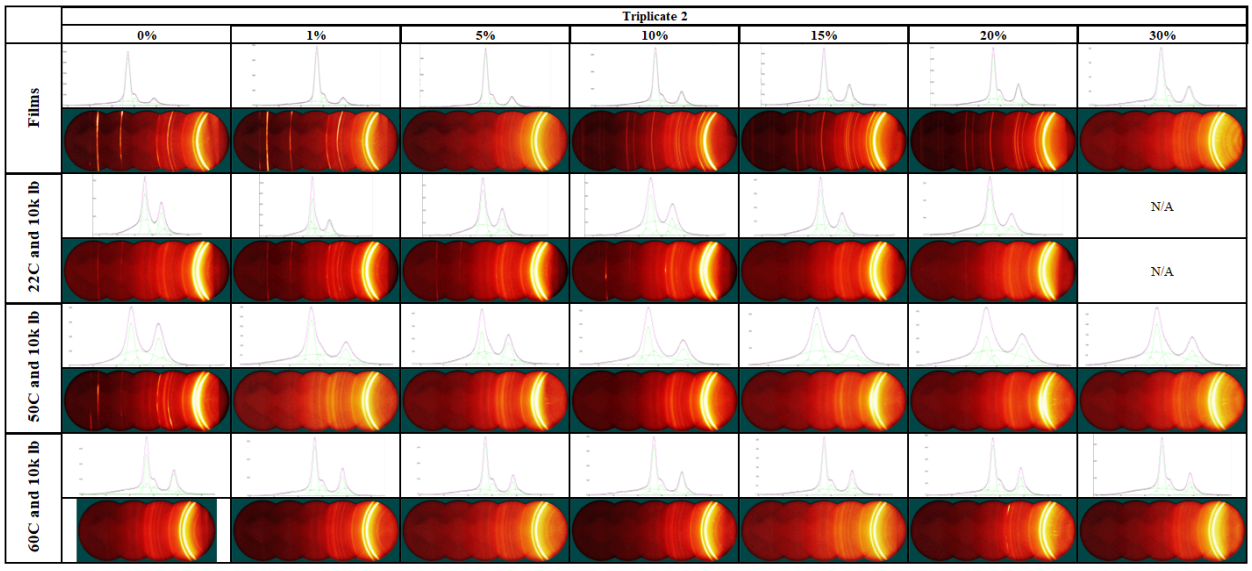

Triplicate 2- Debye Ring and XY Scattering Plots

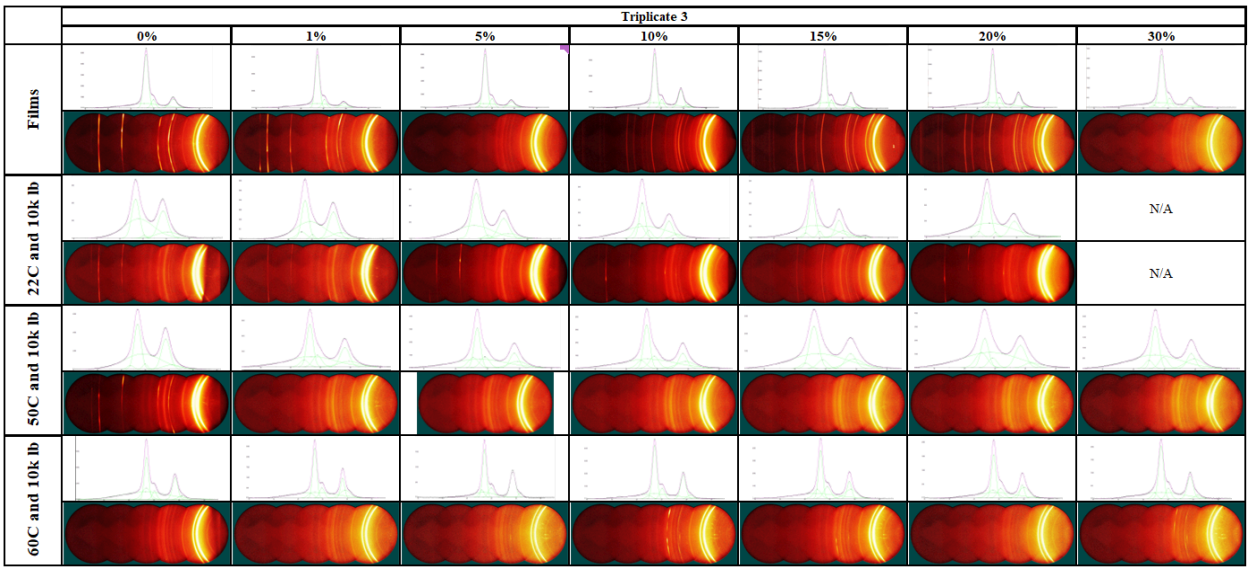

Triplicate 3- Debye Ring and XY Scattering Plots

	Crystallinity		*Amorphous*		*Mesophase*	
Sample Name	*% Avg*	*std dev*	*% Avg*	*std dev*	*% Avg*	*std dev*
0% Film	67.02	4.32	32.98	4.32	0.00	0.00
0% 22C + 10k lb	36.53	4.72	39.65	1.29	23.82	5.97
0% 50C + 10k lb	38.40	1.07	41.87	2.41	19.73	1.71
0% 60C + 10k lb	45.81	6.94	43.16	0.46	11.03	6.47
1% Film	69.55	3.26	30.45	3.26	0.00	0.00
1% 22C + 10k lb	34.28	4.72	38.23	2.92	27.49	0.00
1% 50C + 10k lb	19.95	4.86	43.27	2.59	36.78	4.88
1% 60C + 10k lb	48.06	0.88	36.15	0.86	15.79	0.18
5% Film	69.57	2.37	29.68	2.03	0.76	0.67
5% 22C + 10k lb	30.92	8.62	37.33	6.51	31.75	12.88
5% 50C + 10k lb	28.85	3.85	40.37	7.08	36.13	3.46

5% 60C + 10k lb	58.33	9.45	29.61	7.18	12.06	2.30
10% Film	63.95	3.93	32.84	3.23	3.21	1.82
10% 22C + 10k lb	33.19	4.90	42.25	6.39	24.55	2.14
10% 50C + 10k lb	25.54	4.07	39.12	6.02	35.34	2.45
10% 60C + 10k lb	56.68	5.04	37.21	5.01	6.11	0.28
15% Film	61.32	2.36	35.80	2.57	2.88	1.03
15% 22C + 10k lb	32.55	2.97	40.87	4.98	26.58	7.36
15% 50C + 10k lb	28.93	3.26	44.08	5.61	26.99	4.65
15% 60C + 10k lb	50.48	2.02	35.90	7.50	13.62	9.49
20% Film	60.68	0.59	35.51	0.55	3.82	0.64
20% 22C + 10k lb	28.63	3.93	43.72	2.54	27.64	1.83
20% 50C + 10k lb	26.49	8.18	45.73	7.39	27.78	2.59
20% 60C + 10k lb	51.44	7.48	26.36	4.05	22.20	3.53
30% Film	61.22	3.89	33.07	2.00	5.71	4.70
30% 50C + 10k lb	25.59	5.77	44.21	6.21	30.19	7.12
30% 60C + 10k lb	48.95	7.28	40.06	3.77	10.99	3.51

Deconvolution Data Summary of Phase Composition Average and Standard Deviation